12. Macleod, K. F. *et al.* p53-dependent and independent expression of p21 during cell growth, differentiation, and DNA damage. *Genes Dev.* **9,** 935–944 (1995).
13. Yin, Y., Solomon, G., Deng, C. & Barrett, J. C. Differential regulation of p21 by p53 and Rb in cellular response to oxidative stress. *Mol. Carcin.* **24,** 15–24 (1999).
14. Yin, Y. *et al.* Involvement of p85 in p53-dependent apoptotic response to oxidative stress. *Nature* **391,** 707–710 (1998).
15. De Haan j., B. *et al.* Mice with a homozygous null mutation for the most abundant glutathione peroxidase, Gpx1, show increased susceptibility to the oxidative stress-inducing agents paraquat and hydrogen peroxide. *J. Biol. Chem.* **273,** 22528–22536 (1998).
16. Sun, J., Childress, A. M., Pinswasdl, C. & Jazwinski, S. Divergent roles of RAS1 and RAS2 in yeast longevity. *J. Biol. Chem.* **269,** 18638–18645 (1994).
17. Kennedy, B. K., Austriaco, N. R., Zhang, J. & Guarente, L. Mutation in the silencing gene SIR4 can delay aging in *S. cerevisiae. Cell* **80,** 485–496 (1995).
18. Murakami, S. & Johnson, T. E. A genetic pathway conferring life extension and resistance to UV stress in *Caenorhabditis elegans. Genetics* **143,** 1207–1218 (1996).
19. Larsen, P. L., Albert, P. S. & Riddle, D. L. Genes that regulate both development and longevity in *C. elegans. Genetics* **139,** 1576–1583 (1995).
20. Service, P. M., Hutchinson, E. W., MacKinley, M. D. & Rose, M. R. Resistance to environmental stress in *Drosophila melanogaster* selected for postponed senescence. *Physiol. Zool.* **58,** 380–389 (1985).
21. Lin, Y. J., Seroude, L. & Benzer, S. Extended life-span and stress resistance in the *Drosophila* mutant *methuselah. Science* **282,** 943–946 (1998).
22. Ishi, N. *et al.* A mutation in succinate dehydrogenase cytochrome b causes oxidative stress and ageing in nematodes. *Nature* **394,** 694–697 (1998).
23. Orr, W. C. & Sohal, R. S. Extension of life-span by overexpression of superoxide dismutase and catalase in *D. melanoganster. Science* **263,** 1128–1130 (1994).
24. Marubini, E. & Valsecchi, M. G. *Analysing Survival Data from Clinical Trials and Observational Studies* (Wiley, New York, 1995).
25. Weindruch, R., Walford, R. L., Fligiel, S. & Guthetrie, D. The retardation of aging in mice by dietary restriction: longevity, cancer, immunity and lifetime energy intake. *J. Nutr.* **116,** 641–654 (1986).
26. Weindruch, R. & Walford, R. L. Dietary restriction in mice beginning at 1 year of age: effect on life-span and spontaneous cancer incidence. *Science* **215,** 1415–1417 (1982).
27. Medawar, P. B. Old age and natural death. *Modern Quarterly* **1,** 30–56 (1946).
28. Lithgow, G. J. & Kirkwood, T. B. L. Mechanisms and evolution of aging. *Science* **273,** 80 (1996).
29. Taub, J. *et al.* A cytosolic catalase is needed to extend adult life span in C. *elegans daf-C* and *clk*-1 mutants. *Nature* **399,** 162–166 (1999).
30. Sohal, R. S. & Weindruch, R. Oxidative stress, caloric restriction, and aging. *Science* **273,** 59–63 (1996).

Supplementary Information is available on *Nature*'s World-Wide Web site (http://www.nature.com) or as paper copy from the London editorial office of *Nature*.

Acknowledgements

We thank V. Soares, P. P. DiFiore, K. Helin, L. Bonfini, I. Nicoletti and G. Della Porta for discussions; C. Matteucci, C. Casciari, M. Scanarini and G. Pelliccia for technical help; A. Ventura and A. Cicalese for contributions; and A. Ariesi for secretarial work. We also acknowledge continuous technical and intellectual support from L. Pozzi in conducting animal experiments. E.M. is the recipient of a fellowship from FIRC. This work was supported by A.I.R.C.

Correspondence and requests for materials should be addressed to P.G.P. (e-mail: pgpelicci@ieo.it).

Structural insights into phosphoinositide 3-kinase catalysis and signalling

Edward H. Walker*, Olga Perisic*, Christian Ried*, Len Stephens† & Roger L. Williams*

* *MRC Laboratory of Molecular Biology, MRC Centre, Hills Road, Cambridge CB2 2QH, UK*
† *The Babraham Institute, Babraham, Cambridge CB2 4AT, UK*

Phosphoinositide 3-kinases (PI3Ks) are ubiquitous lipid kinases that function both as signal transducers downstream of cell-surface receptors and in constitutive intracellular membrane and protein trafficking pathways. All PI3Ks are dual-specificity enzymes with a lipid kinase activity which phosphorylates phosphoinositides at the 3-hydroxyl, and a protein kinase activity. The products of PI3K-catalysed reactions, phosphatidylinositol 3,4,5-trisphosphate (PtdIns(3,4,5)P_3), PtdIns(3,4)P_2 and PtdIns(3)P, are second messengers in a variety of signal transduction pathways, including those essential to cell proliferation, adhesion, survival, cytoskeletal rearrangement and vesicle trafficking[1,2]. Here we report the 2.2 Å X-ray crystallographic structure of the catalytic subunit of PI3Kγ, the class I enzyme that is activated by heterotrimeric G-protein βγ subunits and Ras. PI3Kγ has a modular organization centred around a helical-domain spine, with C2 and catalytic domains positioned to interact with phospholipid membranes, and a Ras-binding domain placed against the catalytic domain where it could drive allosteric activation of the enzyme.

The mammalian PI3Ks can be divided into three classes on the basis of their structure and substrate specificity[2]. The class I PI3Ks are receptor-regulated heterodimeric enzymes that preferentially phosphorylate PtdIns(4,5)P_2 *in vivo*. The class IA PI3Ks (consisting of p110α, p110β or p110δ catalytic subunits) associate with a p85 adaptor protein that is essential for interaction of these PI3Ks with receptor tyrosine kinases. The class IB PI3K (PI3Kγ) is activated by heterotrimeric G-protein subunits and associates with a p101 adaptor that is required for full responsiveness to Gβγ heterodimers[3,4]. Class I PI3Ks are also activated by Ras. Class II PI3Ks are distinguished by a carboxy-terminal C2 domain and preferentially use PtdIns and PtdIns(4)P as substrates. Class III enzymes phosphorylate only PtdIns and lack the Ras-binding domain.

We have determined the structure of the catalytic subunit (residues 144–1,102) of porcine PI3Kγ. This construct contains all of the homology regions (HR) found in class I PI3Ks (HR1, HR2, HR3 and HR4) and has a catalytic activity similar to that of the full-length enzyme. The amino-terminal region missing from our construct of PI3Kγ is important for interaction with the p101 adaptor[5], and the analogous region of PI3Kα interacts with the p85 adaptor. The enzyme has a modular structure consisting of four domains: a Ras-binding domain (RBD), a C2 domain, a helical domain and a catalytic domain (Fig. 1). The RBD, C2 and catalytic domains have folds similar to these modules in other proteins involved in signal transduction. The helical domain has a fold akin to HEAT repeat containing structures involved in protein–protein interactions.

The catalytic domain of the enzyme consists of a smaller N-terminal lobe (residues 726–883) and a larger C-terminal lobe (884–1092). The N-terminal lobe from kβ3 to kα3 and the first part of the C-terminal lobe (up to the end of kβ10) have a fold similar to protein kinases (reviewed in ref. 6), and this similarity extends to many of the details of the ATP-binding site (Fig. 2). This region is among the most conserved regions of the PI3Ks (Fig. 3). The structural similarity of PI3K to protein kinases is consistent with PI3Ks having protein kinase activity in addition to their lipid kinase activities[7,8]. The sequence alignment in Fig. 3 shows the regions of PI3K that structurally superimpose with tyrosine protein kinase c-Src. The N-terminal lobe comprises a five-stranded anti-parallel β-sheet flanked on one side by a helical hairpin (kα1–kα2) and a small two-stranded β-sheet (β1–β2), and on the other side by the kα3 helix and the C-terminal lobe. Strands kβ3–kβ7 correspond to the five-stranded β-sheet found in the protein kinases. The kβ3–kβ4 loop corresponds to the protien kinase β1–β2 loop (also known as the glycine-rich or P-loop). This loop interacts closely with the phosphates of the bound ATP, but unlike the protein kinases, it contains no glycine. Instead, the side chain of Ser 806, a residue that is conserved in all PI3Ks, interacts with the β-phosphate (Fig. 2). Lys 833 at the end of kβ5, corresponding to Lys 72 of c-AMP-dependent protein kinase, interacts with the α-phosphate of ATP. This residue is conserved in all PI3Ks and is covalently modified by wortmannin[9]. There are two metal-binding sites (Me; Fig. 2). Me I interacts with the conserved Asn 951, whereas Me II interacts with Asp 836 and Asp 964.

N- and C-terminal lobes are linked through a loop between strands kβ7 and kβ8. This loop forms the deepest wall of the ATP-

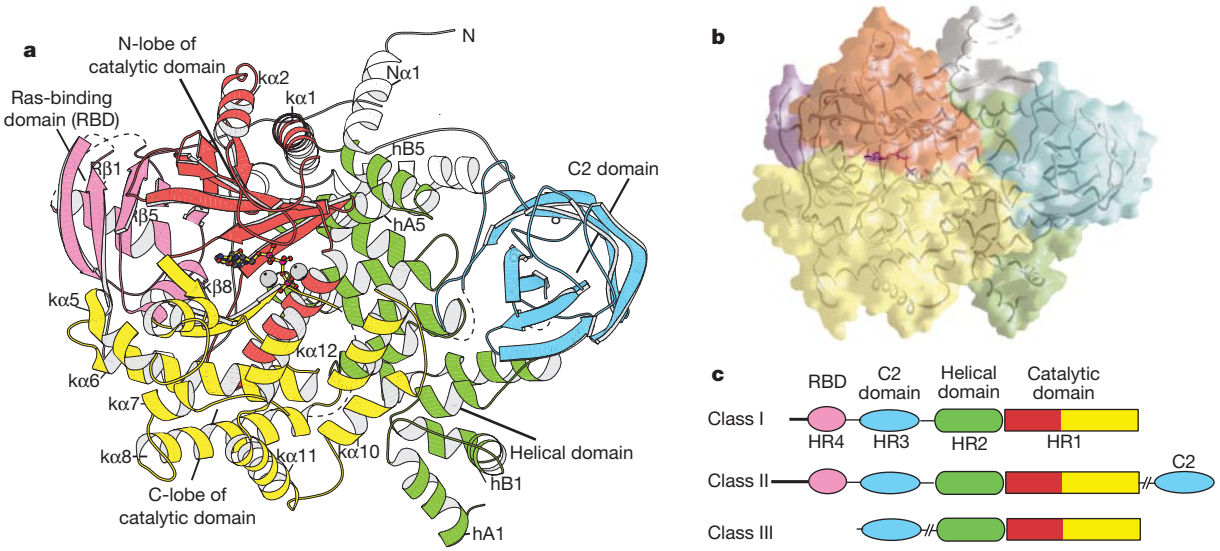

Figure 1 Overall structure of PI3Kγ. **a**, Ribbon diagram of PI3Kγ (prepared with MOLSCRIPT[31]) showing the four domains: RBD (magenta), C2 (blue), helical (green) and catalytic with N-lobe (red) and C-lobe (yellow). The N-terminal region preceding the RBD and the ordered portion between the RBD and C2 domain are white. **b**, The solvent-accessible surface of the enzyme in the same orientation as in **a** (prepared with GRASP[29]). **c**, Domain organization of the PI3K classes.

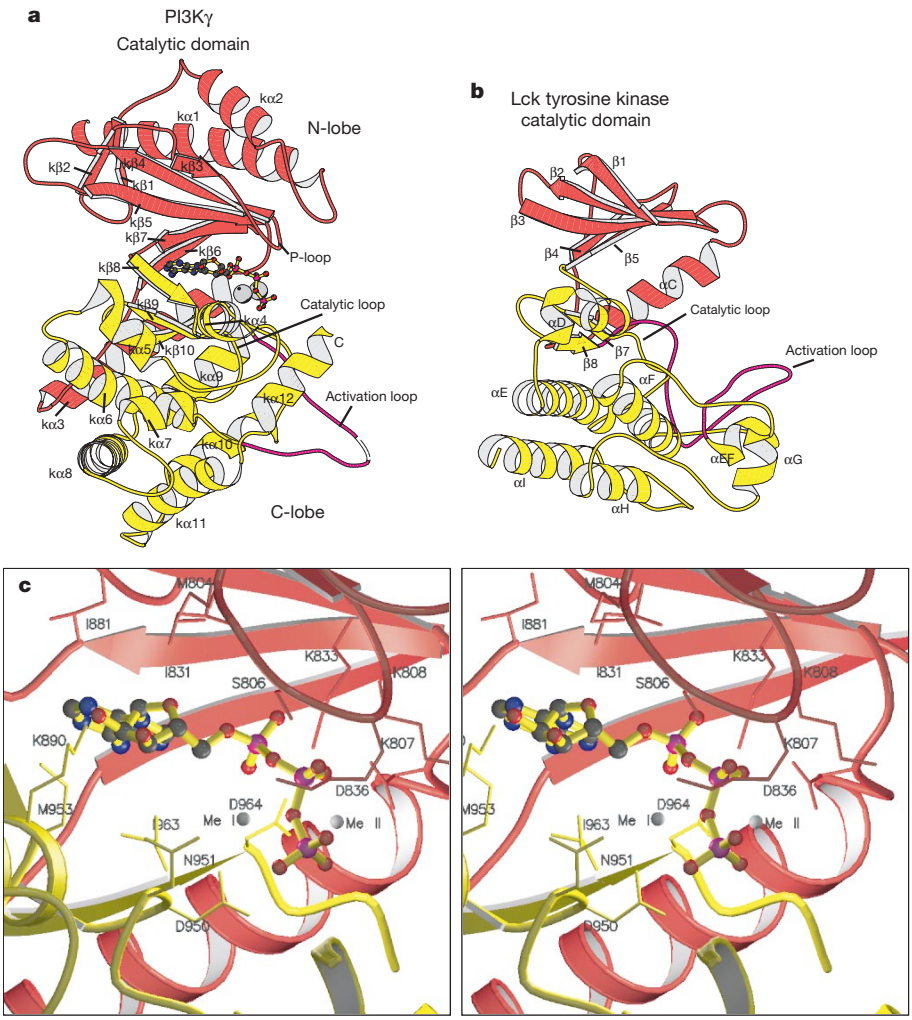

Figure 2 The catalytic domain of PI3Kγ. **a**, Ribbon diagram of the PI3Kγ catalytic domain with bound ATP. The two disordered residues in the middle of the activation loop (magenta) are represented by dotted lines. **b**, The active conformation of the Src family protein kinase Lck[30] (PDB entry 3lck). **c**, Stereo diagram of PI3Kγ active site with bound ATP and two Lu^{3+} ions (Me I and Me II).

binding pocket and provides two hydrophobic contacts with the adenine moiety of the ATP. The C-terminal lobe forms part of the ATP-binding site, as well as the binding site for phospholipid substrates. The region between kα6 and kβ9 (residues 943–951) corresponds to the catalytic loop of the protein kinases; mutations of residues in this loop corresponding to Asp 946, Arg 947, Asp 950 and Asn 951 of PI3Kγ abolish kinase activity of PI3Ks[7,8].

The C-terminal lobe contains a segment (964–988) analogous to the activation loop in the protein kinases; this loop is essential for the substrate specificity of the PI3Ks[10]. In the ATP–Lu^{3+} complex, much of this loop (968–982) is disordered. In the structure of an enzyme/chloramine T complex, all but two residues (Phe 975 and Leu 976) are visible, although high *B*-factors suggest that this loop is flexible. The activation loop is on the surface of the enzyme between the C-terminal helix kα12 on one side and kα10 on the other. We attempted to soak phospholipid analogues into PI3Kγ crystals, but no substrate was evident in the electron density. Consequently, we modelled phospholipid headgroup binding, but because conformational changes probably occur in the activation loop and possibly in the C-terminal helix upon substrate binding, our model is only approximate. In the model, the headgroup is positioned in a cavity lined by the C-terminal helix kα12, the activation loop and the catalytic loop (Fig. 4). This places the 5-phosphate of a PtdIns(4,5)P_2 adjacent to Lys 973 and the I-phosphate near Lys 807 and Lys 808. Lys 973 acting as a ligand of the 5-phosphate may explain why this residue is not found in the class II PI3Ks that do not phosphorylate phosphoinositides with a 5-phosphate. The basic residues nearest the 4-phosphate are Arg 947 and Lys 973. The specificity of the class III PI3Ks for phosphatidylinositol may be explained by their shorter activation loop, which may not leave sufficient space to accommodate a 4-phosphate at the bottom of the headgroup-binding pocket. PI3Kδ autophosphorylates in a region just beyond the C-terminal helix kα12[11], which results in enzyme inhibition probably by sterically preventing substrate binding. The proximity of the C-terminal segment to the substrate-binding site is consistent with autophosphorylation of this region.

The mechanism originally proposed for the enzymatic activity of protein kinases involved a residue acting as a general base to deprotonate the hydroxyl of the substrate and generate a nucleophile that would attack the γ-phosphate of ATP. In cAMP-dependent protein kinase (cAPK), this base has been proposed to be Asp 166, which corresponds to Asp 946 of the PI3Kγ-946-DRH-948 sequence that is conserved in all PI3Ks. In the structure of PI3Kγ, however, Asp 946 is not in a location where it could function as a general base catalyst. The constellation of residues in the active site in the presence of ATP–metal suggests that Asp 946 may simply have a structural role in maintaining the ATP-binding pocket. Therefore, either PI3K has no general base catalyst, in which case the mechanism could be primarily dissociative, involving a metaphosphate transition state[12], or a different residue assumes this function. One possible candidate is His 948; although its side chain is not near the γ-phosphate of ATP, a rotation around $\chi 1$ would place it in a location such that it could interact with the 3-hydroxyl of the lipid headgroup.

PI3Ks are one of the effectors for Ras proteins (reviewed in ref. 13). Binding of PI3K to Ras is affected by mutations in both switch I and switch II regions of Ras (residues 30–38 and 60–76, respectively)[14,15]. These two regions change conformation upon GTP binding and are binding sites for a diverse array of downstream effectors; however, mutations in these switch regions differentially affect the binding of various effectors.

The RBD of PI3Kγ (residues 220–311) has the same fold as the RBD of Raf[16] and RalGDS[17], two other well-characterized effectors of Ras (Fig. 5). The RBD of PI3K consists of a five-stranded mixed β-sheet (Rβ1–Rβ5) flanked by two α-helices (Rα1 and Rα2). Residues 228–230 (in the Rβ1–Rβ2 loop) and 257–265 (in the Rα1–Rβ3 loop) are disordered.

The crystal structure of Ras-related protein Rap1A in complex with the RBD of protein kinase c-Raf[16] and the structure of Ras in complex with the RBD of RalGDS[17] suggest a structural basis for effector specificity. The structures of both of these complexes were determined using the isolated RBD, without the catalytic portions

Table 1 Data collection, structure determination and refinement statistics

Data collection and multiple isomorphous replacement phasing statistics

Data set	Resolution (Å)	Observations/ unique reflections	Completeness (last shell) (%)	R_{merge}‡‡	$\langle I/\sigma \rangle$ (last shell)	No. of sites	Phasing power‖‖	R_{iso}§§
Native*††	2.4	144,973/37,485	97.2 (90.6)	8.5	16.0 (3.1)	–	–	–
$LuCl_3$-1†☆	2.2	191,292/49,599	95.5 (93.3)	9.5	14.3 (1.1)	7	1.7	0.23
$LuCl_3$-2‡††	3.5	43,038/12,484	99.7 (98.2)	8.5	11.3 (3.4)	3	1.9	0.18
Lanthanides§††	3.0	71,426/19,180	97.9 (97.1)	4.5	15.6 (2.3)	8	1.9	0.24
ATM‖††	2.7	94,900/25,688	92.6 (60.2)	4.8	17.0 (5.7)	5	0.8	0.22
Iodine¶†††	2.6	102,511/28,856	93.2 (67.1)	6.0	13.6 (1.4)	3	0.1	0.21

Refinement statistics

Data set	Resolution (Å)	Protein atoms	Waters	R_{cryst}¶¶	R_{free}¶¶ (% data)	R.m.s.d. from ideality##		
						Bonds	Angles	Dihedrals
$LuCl_3$-1	25.0–2.2	6,813	89	0.25	0.30 (5.4)	0.013 Å	1.7°	23°
Iodine¶	25.0–2.6	6,954	14	0.26	0.33 (5.0)	0.005 Å	1.1°	21°
Mn#	25.0–2.6	6,837	26	0.26	0.32 (5.6)	0.005 Å	1.2°	21°

Overall figure of merit 0.45

* The native crystal was soaked in 2.5 mM $InsP_3$, 1.0 mM ATP and 10 mM $MgCl_2$ for 1 h. Although this was the native crystal for heavy-atom phasing, the final high-resolution structure refinement used data from $LuCl_3$-1.
† $LuCl_3$-1 crystal was soaked in 20 mM $LuCl_3$ and 1.25 mM ATP for 1 h 40 min.
‡ $LuCl_3$-2 crystal was soaked in 20 mM $LuCl_3$ and 1.3 mM ATP for 4 h.
§ Lanthanides crystal was soaked for 4 h in a mixture of 3.3 mM each of $GdCl_3$, $TbCl_3$, $HoCl_3$, $ErCl_3$, $TmCl_3$, and $LuCl_3$ with 1.26 mM ATP and 1 mM EMTS.
‖ ATM crystal was soaked for 22 h in 10 mM sodium aurothiomalate.
¶ Iodine crystal was soaked for 75 min in 1 mM NaI_3 and 1 mM chloramine T. This crystal was originally prepared in an attempt to iodinate tyrosine residues as a heavy atom derivative, but no evidence of tyrosine iodination was seen in the resulting structure.
# Mn crystal contained 1.4 mM ATP and 14 mM $MnCl_2$.
☆ Data were collected at ESRF beamline ID2b.
†† Data were collected at ESRF beamline ID14-4.
‡‡ $R_{merge} = \Sigma_{hkl}\Sigma_i|I_i(hkl) - \langle I(hkl)\rangle|/\Sigma_{hkl}\Sigma_i I_i(hkl)$.
§§ $R_{iso} = \Sigma||F_{deriv}| - |F_{native}||/\Sigma|F_{native}|$.
‖‖ The phasing power is defined as the ratio of the r.m.s. value of the heavy atom structure factor amplitudes and the r.m.s. value of the lack-of-closure error.
¶¶ R_{cryst} and $R_{free} = \Sigma|F_{obs} - F_{calc}|/\Sigma F_{obs}$; R_{free} calculated with the percentage of the data shown in parentheses.
R.m.s. deviations for bond angles and lengths in regard to Engh and Huber parameters.

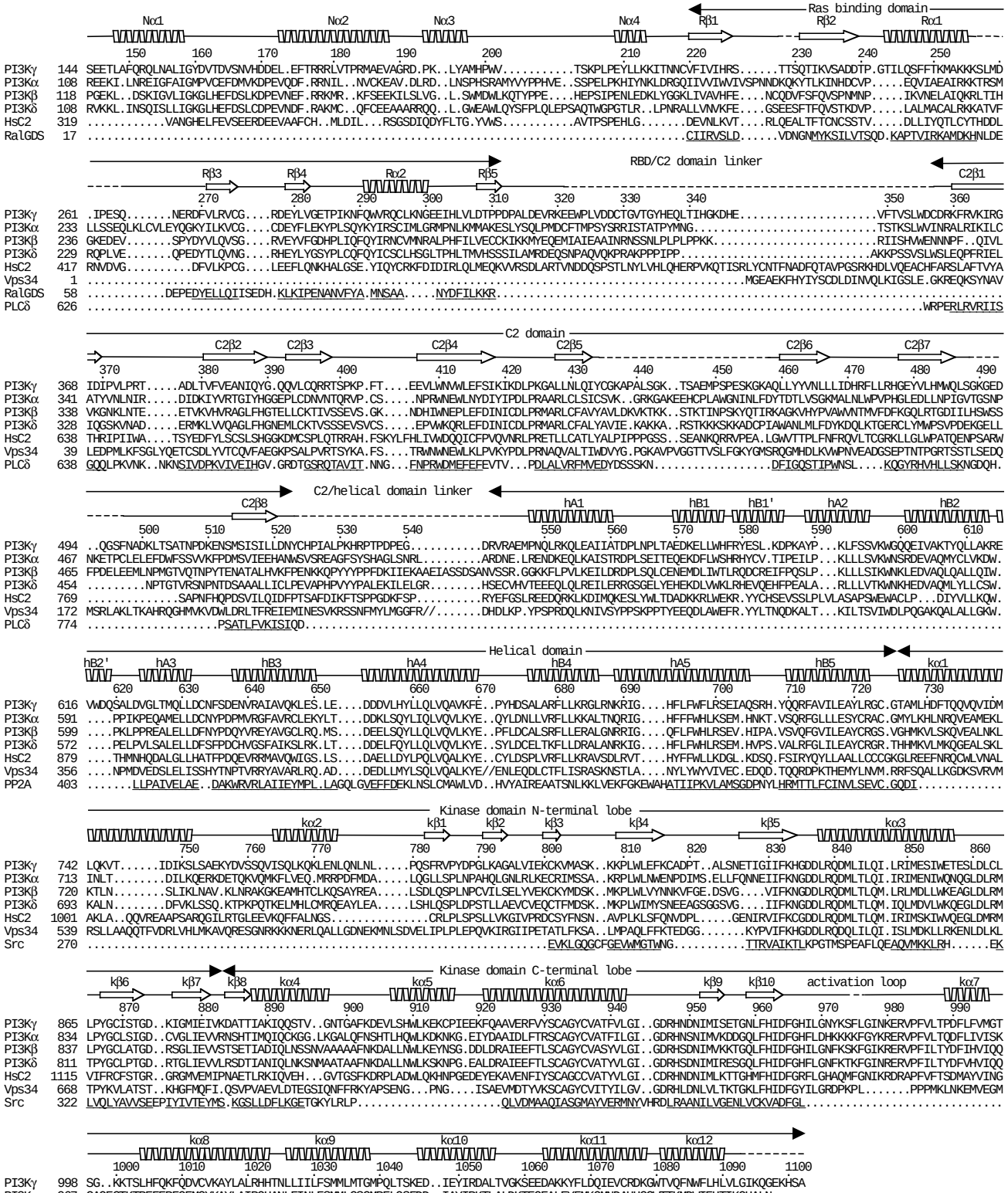

Figure 3 Secondary structure of the PI3K-γ p110 subunit and sequence alignments with other PI3K family members. Alignments are based on the Pfam database. The last line of the alignment illustrates proteins with structurally similar domains. Residues that superimpose with PI3K-γ are underlined. Sequences are porcine PI3K-γ (o02697), human PI3Kα (p42336), human PI3Kβ (p42338), human PI3Kδ (o00329), human class II PI3K (HsC2-PI3K, o00750), human Vps34 (s57219), RalGDS (1lfd), phospholipase Cδ (1djx), PR65/A regulatory subunit (1b3u) and tyrosine kinase c-Src (1fmk). Dashed lines in the secondary structure indicate disordered residues and // indicates a large gap in the sequence.

of the effector molecules. The PI3Kγ structure shows how the RBD interacts with the rest of the enzyme. The RBD of PI3Kγ contacts the N-lobe and to a lesser degree the C-lobe of the catalytic domain. Residues in Rα2 and the Rβ3–Rβ4 loop interact with the catalytic domain, mainly with the kβ1–kβ2 and kβ4–kβ5 loops and helix kα6. The relationship of the RBD to the rest of the enzyme suggests two possible mechanisms by which Ras binding may cause effector activation: a recruitment mechanism, in which Ras increases PI3K activity by translocating the enzyme to the plasma membrane; and an allosteric mechanism, in which Ras binding to the RBD causes a conformational change that would be propagated through the RBD/catalytic domain interface to affect substrate or cofactor binding.

By superimposing the RBDs of RalGDS and PI3Kγ, we constructed a model of Ras interaction with PI3Kγ (Fig. 5) from which we can rationalize the differential effects of various switch I and switch II mutants on PI3K binding compared with other effectors. T35S and D38E mutations in Ras switch I eliminate PI3K binding, but do not affect Raf binding[15]. The E37G mutation abolishes binding to PI3K and Raf but not to RalGDS. The Y40C mutation does not affect PI3K binding, but abrogates Raf and RalGDS binding. In the switch II region, the Y64G mutation eliminates PI3K and neurofibromin binding but has no effect on Raf binding[14].

In our model of the PI3K–Ras interaction, residues Glu 37, Asp 38, Tyr 40 and Tyr 64 are at the PI3K–Ras interface. Lys 234 of PI3K could form a salt bridge to Glu 37 of Ras and Lys 255 at the C-terminal end of Rα1 could form a salt bridge with Asp 38 of Ras. Lys 255 at the C-terminal end of Rα1 could form a salt bridge with Asp 38 of Ras. Lys 255 in PI3Kγ is probably analogous to Lys 227 in PI3Kα, in which mutation K227E blocks PI3Kα binding to Ras[15]. Tyr 40 interacts with Lys 32 in RalGDS (numbering as in ref. 17); however, the very different orientation of the Lys 32 equivalent in PI3Kγ (Lys 234) may not allow this interaction, which may account for the insensitivity of PI3K to the Y40C mutation. On the other hand, Tyr 64 in switch II is in a position to form a hydrogen bond with PI3K Asp 238, but this residue has no specific interaction with RalGDS, which may explain the sensitivity of PI3K to the Ras Y64G mutation.

The PI3Kγ C2 domain (residues 357–522) is an eight-stranded antiparallel β-sandwich consisting of two four-stranded β-sheets (Fig. 6). The fold of this domain is the same as the type II C2 domain found in PLCδ1[18]. The N-terminal regions of all three PI3K classes have C2 domains, whereas the class II enzymes have an additional C2 domain at the C terminus (Fig. 1). The segments leading from the RBD into the C2 domain and from the C2 domain to the helical domain are not ordered.

C2 domains are often involved in Ca^{2+}-dependent or Ca^{2+}-independent phospholipid membrane binding using three loops known as CBRs located at one end of the domain. The CBRs for PI3Kγ are the loops connecting β1 with β2 (CBR1), β3 with β4 (CBR2), and β5 with β6 (CBR3). The CBR3 of PI3Kγ is quite long compared with other C2 domains and is disordered in our structure.

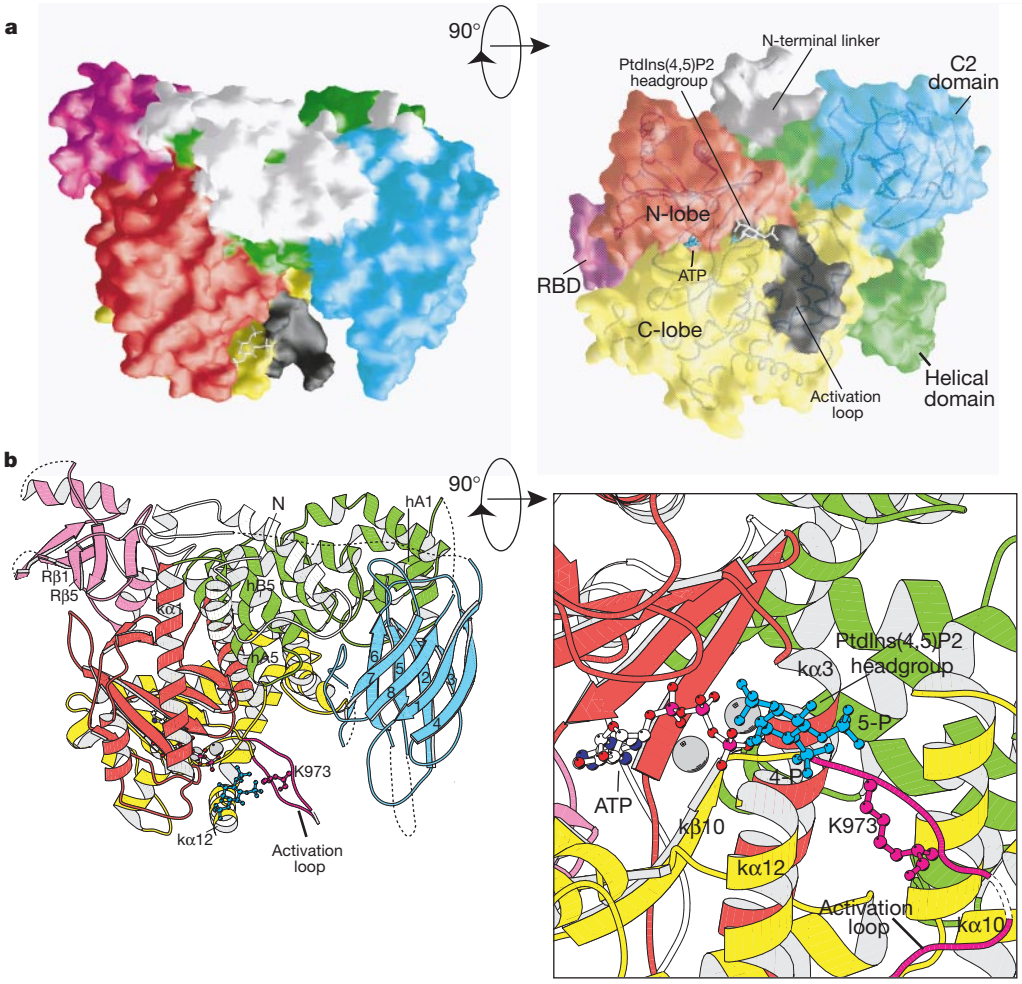

Figure 4 Model of phospholipid headgroup interactions with PI3Kγ. **a**, Orthogonal views of the solvent-accessible surface. The activation loop is black. An inositol 1,4,5-trisphosphate ($InsP_3$) molecule (white ball-and-stick) is modelled in the active site with the 3-OH near the γ-phosphate of the bound ATP. **b**, The same views in ribbon representation showing the activation loop (magenta) and $InsP_3$ (blue). The right panel is expanded to show features of the putative headgroup interaction.

The C2 domain interacts primarily with the helical domain, but it also interacts with the linker segment before the RBD and with the C-terminal lobe of the catalytic domain. The surface of the C2 domain contacting the rest of PI3Kγ is nearly identical to the surface of the PLCδ1 C2 domain that contacts the catalytic domain of PLCδ1.

PI3K can bind phospholipid membranes in the absence of other protein components in a Ca^{2+}-independent manner and can carry out processive catalysis at the membrane surface. By analogy with enzymes such as protein kinase C and cytosolic phospholipase A2, the C2 domain of PI3K may participate in membrane interaction. Consistent with this, we found that the isolated C2 domain from PI3Kγ binds multilamellar phospholipid vesicles similarly to the full-length enzyme (data not shown). In PI3Kβ and PI3Kδ, CBR3 (residues 395–417 of PI3Kδ) is particularly rich in basic residues that may be important for membrane binding.

The structure of a type IIβ phosphatidylinositol phosphate kinase (PIPK) has been reported[19]. This dimeric enzyme, which phosphorylates phosphoinisitides at the 4-hydroxyl, consists of a single, catalytic domain. The dimer has an extensive flat, positively charged surface which was proposed to be the membrane-binding interface of the enzyme. Although the N-lobe of PIPK is structurally related to the catalytic domain of PI3Kγ, the location of PI3Kγ C2 domain with respect to the catalytic domain sterically precludes membrane interactions using the surface of PI3Kγ analogous to the putative PIPK membrane-binding surface. Given the location of the membrane-binding loops from the C2 domain and the cavity in the catalytic domain that must accommodate the PtdIns(4,5)P_2

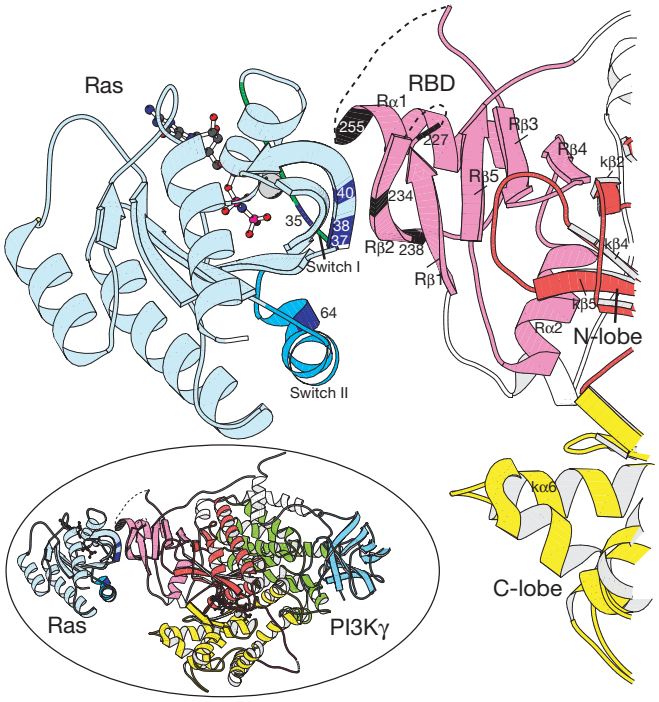

Figure 5 Model of the Ras–PI3Kγ interaction based on the structure of the RalGDS–Ras complex. Inset, overall view of Ras–PI3Kγ interaction. Residues in Switch I (green) and Switch II (cyan) regions of Ras that influence effector binding are highlighted with dark blue stripes, whereas residues in the RBD of PI3K (purple) that are likely to be involved in Ras binding are shown as black stripes. Note the proximity of the RBD to the two lobes of the catalytic domain.

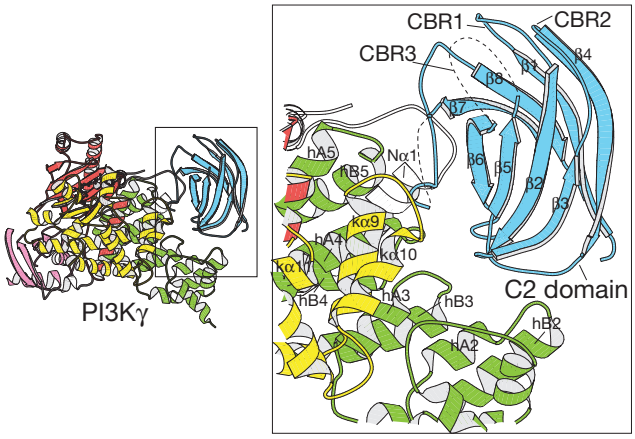

Figure 6 Ribbon diagram of the PI3Kγ C2 domain, and the interactions it makes with the rest of the enzyme. The elements of the helical and catalytic domains interacting with the C2 domain are shown. The domain in relation to the whole enzyme is shown to the left.

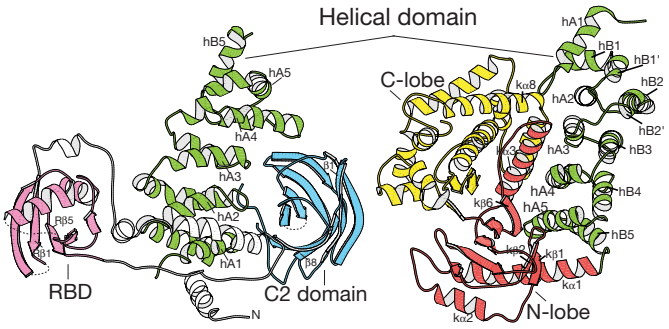

Figure 7 The helical domain (for colours see Fig. 1). The A/B antiparallel helical pairs characteristic of the HEAT motif topology consist of hA1/hB1, hA2/hB2, hA3/hB3, hA4/hB4 and hA5/hB5. Left, interaction between the helical domain and the RBD and C2 domain (the rest of the protein is removed for clarity). This interaction involves principally the A-helix surfaces. Right, interactions between the helical domain and the catalytic domain.

headgroup, the membrane-binding surface of PI3Kγ could consist of the CBRs, the crevice between the N- and C-lobes of the catalytic domain, and the tip of the activation loop (Fig. 4a, right panel represents a view from the membrane surface).

The helical domain of PI3K (545–725) consists of five A/B pairs of anti-parallel helices (Fig. 7). The first two pairs have one kinked helix each, hB1/hB1′ and hB2/hB2′. This region has been variously referred to as HR2, the PI3K accessory domain and the PIK domain, but its function is not known. The paired arrangement of a series of helices connected into a right-handed superhelix is reminiscent of the PR65/A regulatory subunit of protein phosphatase 2A (PP2A)[20]. PR65/A is a member of a diverse group of proteins that contain 3–25 tandem repeats of a short sequence, called the HEAT motif. The HEAT motif consists of paired helices A and B arranged so that the A and B helices within a pair are antiparallel, and the A and B helices from one motif are parallel to the A and B helices of the next motif in the sequence. Although no HEAT sequence motif is apparent in the helical domain of PI3K, its structure is quite similar to that of PR65/A in terms of the arrangement of helices, the length of the A/B units, and the angle between the A/B pairs.

The function of HEAT repeats is to form protein–protein interactions. In importin-β, interactions with the small GTPase Ran involve the surfaces of the B helices[21]. In PR65/A, mutagenesis has implicated the loops connecting the A/B pairs as the region responsible for interaction with PP2A[20]. In PI3Kγ, the helical domain is central to the interdomain packing: the surface formed by the A helices interacts with the catalytic domain; the loops connecting A and B helices within a pair pack against the C2 domain; and the loops between helical pairs pack against the RBD (Fig. 7). Much of the 'B' surface is solvent exposed and may interact with other proteins that bind PI3Kγ, such as the p101 adaptor or Gβγ subunits.

The helical domain is common to both PI3K and PI4K families and serves as a spine on which the other domains are fastened. One of the proteins in which the HEAT sequence motif was first noted is the target of rapamycin, TOR, a yeast homologue of human FRAP (reviewed in ref. 22). FRAP has a C-terminal domain with clear sequence homology to the catalytic domain of PI3Ks. The secondary-structure prediction for the remainder of FRAP suggests that most of FRAP, apart from the catalytic domain, may consist of helical repeats folded into a right-handed superhelix as in the helical domain of PI3Kγ.

This first structure of a PI3K provides a framework within which mutagenesis and detailed kinetic studies can be carried out to establish the enzymatic mechanism and the mode of activation by Ras and heterotrimeric G-protein subunits. □

Methods

Protein expression, purification and crystallization

The cell-free extract of baculovirus-infected Sf9 cells expressing the His-tagged catalytic subunit of porcine PI3Kγ (residues 1–143 deleted) was used for protein purification using Talon resin, followed by thrombin cleavage, anion and cation exchange, and gel filtration chromatography. Crystals were grown by mixing 1 μl of PI3K (3.5–4.0 mg ml^{-1}, in a buffer containing 20 mM Tris-HCl pH7.2, 1% v/v ethylene glycol, 1% w/v betaine, 0.02% w/v CHAPS and 5 mM dithiothreitol) with 1 μl of a reservoir solution containing 150–200 mM Li_2SO_4, 100 mM Tris-HCl pH 7.25 and 14–15% PEG 4000.

Data collection and structure determination

Crystals have C2 symmetry with unit-cell dimensions of $a = 143.3$ Å, $b = 67.6$ Å, $c = 107.0$ Å, $\beta = 95.9°$, and contain one protein molecule in the asymmetric unit. Diffraction data were collected at ESRF beamlines ID2 and ID14-4 at 100K after freezing crystals in a cryoprotectant consisting of 150–200 mM Li_2SO_4, 100 mM Tris-HCl pH 7.25, 12% glycerol and 20% PEG 4000. Data were processed using MOSFLM[23] and CCP4 programs[24]. The structure was determined by multiple isomorphous replacement methods. Heavy-atom positions were located using Solve[25] and refined with Sharp[26] (Table 1). A model was built into the electron-density maps using the program O[27] and refined using CNS[28]. The average *B*-factor for all atoms is 60 $Å^2$. The structure has no residues in disallowed regions of the Ramachandran plot.

The highest resolution data obtained were for the complex containing ATP and lutetium; refinement resulted in a model with a free *R*-factor of 0.30 to a resolution of 2.2 Å. This complex has 854 residues visible in the electron-density map. Crystals with and without ATP had only minor differences in side-chain conformations in the active-site residues. PI3Ks require a Mg^{2+} or Mn^{2+} cofactor for enzymatic activity. In complexes with Lu^{3+}, Mg^{2+} or Mn^{2+}, each of the metals binds at the same two sites.

Received 10 August; accepted 6 October 1999.

1. Toker, A. & Cantley, L. C. Signalling through the lipid products of phosphoinositide-3-OH kinase. *Nature* **387,** 673–676 (1997).
2. Domin, J. & Waterfield, M. D. Using structure to define the function of phosphoinositide 3-kinase family members. *FEBS Lett.* **410,** 91–95 (1997).
3. Stoyanov, B. *et al.* Cloning and characterisation of a G protein-activated human phosphoinositide-3 kinase. *Science* **269,** 690–693 (1995).
4. Stephens, L. R. *et al.* The Gβγ sensitivity of a PI3K is dependent upon a tightly associated adaptor, p101. *Cell* **89,** 105–114 (1997).
5. Krugmann, S., Hawkins, P. T., Pryer, N. & Braselmann, S. Characterizing the interactions between the two subunits of the p101/p110γ phosphoinositide 3-kinase and their role in the activation of this enzyme by Gβγ subunits. *J. Biol. Chem.* **274,** 17152–17158 (1999).
6. Taylor, S. S. *et al.* Catalytic subunit of cyclic AMP-dependent protein kinase: structure and dynamics of the active site cleft. *Pharmacol. Ther.* **82,** 133–141 (1999).
7. Dhand, R. *et al.* PI3-kinase is a dual specificity enzyme—autoregulation by an intrinsic protein serine kinase activity. *EMBO J.* **13,** 522–533 (1994).
8. Stack, J. H. & Emr, S. D. Vps34p required for yeast vacuolar protein sorting is a multiple specificity kinase that exhibits both protein kinase and phosphatidylinositol-specific PI-3-kinase activities. *J. Biol. Chem.* **269,** 31552–31562 (1994).
9. Wymann, M. P. *et al.* Wortmannin inactivates phosphoinositide 3-kinase by covalent modification of Lys-802, a residue involved in the phosphate transfer reaction. *Mol. Cell. Biol.* **16,** 1722–1733 (1996).
10. Bondeva, T. *et al.* Bifurcation of lipid and protein kinase signals of PI3Kγ to the protein kinases PKB and MAPK. *Science* **282,** 293–296 (1998).
11. Vanhaesebroeck, B. *et al.* Autophosphorylation of p110δ phosphoinositide 3-kinase: a new paradigm for the regulation of lipid kinases *in vitro* and *in vivo*. *EMBO J.* **18,** 1292–1302 (1999).
12. Kim, K. & Cole, P. A. Measurement of a Brønsted nucleophile coefficient and insights into the transition state for a protein tyrosine kinase. *J. Am. Chem. Soc.* **119,** 11096–11097 (1997).
13. Marshall, C. J. Ras effectors. *Curr. Opin. Cell Biol.* **8,** 197–204 (1996).
14. Moodie, S. A. *et al.* Different structural requirements within the switch II region of the Ras protein for interactions with specific downstream targets. *Oncogene* **11,** 447–454 (1995).
15. Rodriguez-Viciana, P. *et al.* Role of phosphoinositide 3-OH kinase in cell transformation and control of the actin cytoskeleton by Ras. *Cell* **89,** 457–467 (1997).
16. Nassar, M. *et al.* the 2.2 Å crystal structure of the Ras-binding domain of the serine/threonine kinase c-Raf1 in complex with Rap1A and a GTP analogue. *Nature* **375,** 554–560 (1995).
17. Huang, L., Hofer, F., Martin, G. S. & Kim, S.-H. Structural basis for the interaction of Ras with RalGDS. *Nature Struct. Biol.* **5,** 422–426 (1998).
18. Essen, L.-O., Perisic, O., Lynch, D. E., Katan, M. & Williams, R. L. A ternary metal binding site in the C2 domain of phosphoinositide-specific phospholipase C-δ1. *Biochemistry* **36,** 2753-2762 (1997).
19. Rao, V. D., Misra, S., Boronenkov, I. V., Anderson, R. A. & Hurley, J. H. Structure of type IIβ phosphatidylinositol phosphate kinase: a protein kinase fold flattened for interfacial phosphorylation. *Cell* **94,** 829–839 (1998).
20. Groves, M. R., Hanlon, N., Turowski, P., Hemmings, B. A. & Barford, D. The structure of the protein phosphatase 2A PR65/A subunit reveals the conformation of its 15 tandemly repeated HEAT motifs. *Cell* **96,** 99–110 (1999).
21. Vetter, I. R., Arndt, A., Kutay, U., Görlich, D. & Wittinghofer, A. Structural view of the Ran-importin β interaction at 2.3 Å resolution. *Cell* **97,** 635–646 (1999).
22. Dennis, P. B., Fumagalli, S. & Thomas, G. Target of rapamycin (TOR): balancing the opposing forces of protein synthesis and degradation. *Curr. Opin. Genet. Dev.* **9,** 49–54 (1999).
23. Leslie, A. G. W. Recent changes to the MOSFLM package for film and image plate data, in *Joint CCP4 and ESF-EACMB Newsletter on Protein Crystallography* Vol. 26 (Daresbury Laboratory, Warrington, UK, 1992).
24. CCP4. Collaborative Computing Project 4: A suite of programs for protein crystallography. *Acta Crystallogr. D* **50,** 760–763 (1994).
25. Terwilliger, T. C. & Berendzen, J. Automated structure solution for MIR and MAD. *Acta Crystallogr. D* **55,** 849–861 (1999).

26. de La Fortelle, E. & Bricogne, G. Maximum-likelihood heavy-atom parameter refinement for multiple isomorphous replacement and multiwavelength anomalous diffraction methods. *Methods Enzymol.* **276,** 472–494 (1997).
27. Jones, T. A., Zou, J.-Y., Cowan, S. W. & Kjeldgaard, M. Improved methods for building protein models in electron density maps and the location of errors in these models. *Acta Crystallogr. A* **47,** 110–119 (1991).
28. Brünger, A. T. *et al.* Crystallography & NMR system: a new software suite for macromolecular structure determination. *Acta Crystallogr. D* **54,** 905–921 (1998).
29. Nicholls, A., Sharp, K. A. & Honig, B. Protein folding and association: insights from the interfacial and thermodynamic properties of hydrocarbons. *Proteins Struct. Funct. Genet.* **11,** 281–296 (1991).
30. Yamaguchi, H. & Hendrickson, W. A. Structural basis for the activation of human lymphocyte kinase Lck tyrosine phosphorylation. *Nature* **384,** 484–489 (1996).
31. Kraulis, P. J. MOLSCRIPT: A program to produce both detailed and schematic plots of protein structures. *J. Appl. Crystallogr.* **24,** 946–950 (1991).

Acknowledgements

We thank D. Lynch for technical assistance, S. Krugmann for PI3K assays, the staff of synchrotron beamlines ID2b, ID14-3 and ID14-4 at ESRF, IMCA-CAT at APS, X11 at EMBL Hamburg, Station 9.6 at Daresbury SRS, and Elettra, Italy, for help in synchrotron data collection. We thank P. Roversi and G. Bricogne for their assistance with BUSTER, R. Rubin and C. Humblet for access to the IMCA-CAT beamline, and P. Hawkins and A. Murzin for helpful discussions. C.R. was supported by the Deutsche Forschungsgemeinschaft. We are grateful for support from the BBSRC (via a senior fellowship to P. Hawkins), the British Heart Foundation, Parke-Davis and Onyx Pharmaceuticals (R.L.W.).

Correspondence and requests for materials should be addressed to R.L.W. (e-mail: rlw@mrc-lmb.cam.ac.uk). The accession code for the atomic coordinates of the structure at the Protein Data Bank is 1qmm.

Sustained oscillations in living cells

Sune Danø, Preben Graae Sørensen & Finn Hynne

Department of Chemistry and CATS, H.C. Ørsted Institute, University of Copenhagen, Universitetsparken 5, DK-2100 Copenhagen, Denmark

Glycolytic oscillations in yeast have been studied for many years simply by adding a glucose pulse to a suspension of cells and measuring the resulting transient oscillations of NADH[1–12]. Here we show, using a suspension of yeast cells, that living cells can be kept in a well defined oscillating state indefinitely when starved cells, glucose and cyanide are pumped into a cuvette with outflow of surplus liquid. Our results show that the transitions between stationary and oscillatory behaviour are uniquely described mathematically by the Hopf bifurcation[13]. This result characterizes the dynamical properties close to the transition point. Our perturbation experiments show that the cells remain strongly coupled very close to the transition. Therefore, the transition takes place in each of the cells and is not a desynchronization phenomenon. With these two observations, a study of the kinetic details of glycolysis, as it actually takes place in a living cell, is possible using experiments designed in the framework of nonlinear dynamics. Acetaldehyde is known to synchronize the oscillations[10]. Our results show that glucose is another messenger substance, as long as the glucose transporter is not saturated.

The ubiquitous glycolytic pathway is the first step in sugar catabolism, producing ATP, NADH and pyruvate. Under anaerobic conditions, the NADH is reused in the subsequent fermentation of the pyruvate. Transient glycolytic oscillations are known to occur in suspensions of yeast cells[1,2]; see ref. 12 for measurements of most of the relevant metabolites during oscillatory glycolysis. The observed bulk oscillations of intracellular NADH depend on the ability of individual cells to synchronize their oscillations. This capability was proven by mixing two suspensions oscillating 180° out of phase: the bulk oscillations of NADH disappear immediately after the mixing, but reappear spontaneously after some time[3,4,10].

Synchronized bulk oscillations depend on a sufficiently high cell density[6]. They are promoted by anaerobiosis, especially when induced by cyanide[4,9], which is a potent inhibitor of cytochrome *c* oxidase in the respiratory chain.

Glycolytic oscillations are normally induced by a pulse of glucose, and the resulting oscillations change gradually as the excess of extracellular glucose is used up. An attempt was made to extend the duration of the oscillations using an infusion system where glucose was slowly injected into the cell suspension[14]. However, owing to cell ageing, accumulation of waste products or dilution of the suspension, the observed oscillations were still transient. In both the infusion experiment and the glucose-pulse experiment, the duration of the oscillating transient depends on the enzymatic composition of the yeast cells[3,7,8,14]. In the glucose-pulse experiments, the longest transient trains of oscillations are found when a saturated, high-affinity glucose transporter provides the cell with an almost constant flow of glucose throughout the transient[11]. In our experimental setup, a continuous-flow stirred tank reactor (CSTR), we control the glycolytic flow by means of the inflows, to give truly sustained oscillations.

To obtain these oscillations, we prepare *Saccharomyces cerevisiae* as described in ref. 8. The yeast is grown in batch culture at 30 °C to the point of glucose depletion. The cells are then removed from the growth medium and starved for a couple of hours, before being resuspended in phosphate buffer and kept below 5 °C. The resulting suspension flows into a stirred and thermostat-regulated reactor through a peristaltic pump. Solutions of glucose and cyanide flow into the reactor through two stepper–motor controlled piston burettes (Fig. 1). We monitor the oscillations by measuring NADH fluorescence.

Figure 2 shows a typical recording of stable undamped oscillations in the cell suspension. In principle the oscillations could continue forever with constant amplitude and period. This is possible because our setup is a truly open system. In practice, the amount of yeast cells available from the batch growth limits the duration of the run to 14 h in our experiments.

The environmental conditions of the cells can be changed by altering the flow rates of the inflows. Depending on flow rate we observe either a stationary state or continuous oscillations. The flow rate where the stationary state becomes unstable is known as the bifurcation point. As the flow rate is changed from this critical value, the amplitude of the oscillations grows in proportion to the square root of the deviation from the critical value. For a dynamic system such behaviour is characteristic of a supercritical Hopf bifurcation (SHB). This description is, of course, only valid sufficiently close to the bifurcation point. In Fig. 3 we show how the amplitude varies with the glucose flow rate. A similar agreement with bifurcation theory is seen when the flow rate of cyanide is

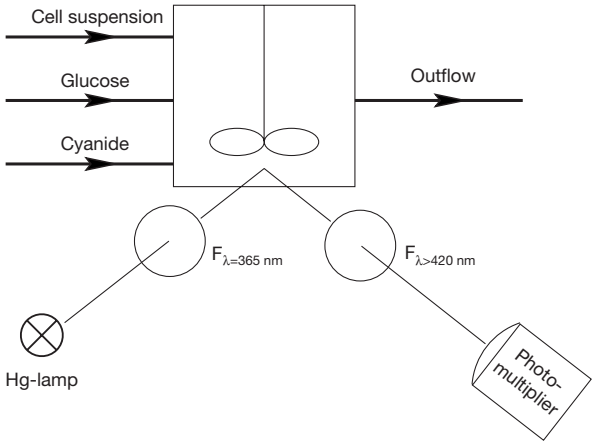

Figure 1 The experimental setup. F designates optical filters. See details in the Methods section.